The importance of advection for CO_2 dynamics in the karst Critical Zone: an approach from dimensional analysis

Matthew D. Covington[1]

[1]*Department of Geosciences, University of Arkansas, Fayetteville, Arkansas, 72701, USA*

ABSTRACT

Karst landscapes provide unique challenges and opportunities to studies of processes within the Critical Zone, which spans from the top of the canopy to the base of active groundwater circulation. Dimensional analysis using the characteristic length scales and times scales of karst processes enables development of an initial framework for quantification of the rates and distribution of these processes throughout the Critical Zone. In particular, dimensional analysis provides a useful tool to identify the relative importance of different processes and to test the assumptions behind models of Critical Zone function. I briefly review prior use of dimensional analysis to understand various aspects of the karst Critical Zone and then introduce simple models for CO_2 transport within fractures and conduits of the vadose zone. Dimensional analysis of these models suggests that advection through karst fractures within both the gas and liquid phases will strongly impact vertical CO_2 profiles in the vadose zone in a variety of settings. Implications of this finding for karst Critical Zone development and future data campaigns are discussed.

INTRODUCTION

The Critical Zone (CZ) spans from the top of the canopy to the base of active groundwater circulation (Brantley et al., 2006). Though an understanding of CZ processes is crucial to predicting how Earth's surface will respond to climate change and anthropogenic impacts, and to unraveling the connections between the physical, chemical, and biological processes that drive landscape evolution, CZ processes and the coupling between them remain relatively poorly understood. This has led to recent efforts toward a general and systematic approach to CZ research as spearheaded by the Critical Zone Exploration Network (CZEN), a network of field sites and community of researchers focused on understanding CZ processes.

Karst landscapes, which form in settings with highly soluble lithologies and occupy roughly 12% of Earth's surface (Ford and Williams, 2007), provide an end-member case of CZ dynamics. In contrast to other settings, karst systems evolve largely by congruent weathering. Additionally, karst systems allow extremely rapid infiltration of water and the solutes and particles transported by water. In karst settings, it is possible to have freshly recharged and chemically aggressive water circulating at depths of hundreds or even thousands of meters within minutes to hours after leaving the surface. One of the challenges of understanding CZ processes is that they span many orders of magnitude in timescales (Brantley et al., 2006). This is exacerbated in karst systems where hydraulic conductivities, and corresponding flow timescales, span over 10 orders of magnitude depending upon the length scale over which they are measured (Worthington, 2009). One advantage to karst CZ research is that, in many cases, the conduit flow network that drains much of the CZ is physically accessible to humans in the form of caves. Despite karst's unique position within the range of Earth's CZ dynamics, and relatively widespread global distribution, a karst field site is not represented within the current CZEN, and karst CZ dynamics are arguably even more poorly understood than other settings.

The preferential flow paths of dissolutionally enlarged fractures and conduits are of central importance to understanding the dynamics of the karst CZ as they largely control the distribution of water flow throughout the CZ and are the locations where geomorphic work is focused. The distribution and apertures of such paths, and their ability to transmit fluids and weathering products, will largely determine the nature of the karst landscape. Many processes occurring within the CZ are controlled by gradients in temperature, solute concentration, carbon dioxide, and the availability of dissolved and particulate organic matter. To understand the variability of these quantities with depth, and as a function of flow path properties, the concept of a process length scale is a useful tool. If a given process that occurs over a characteristic time scale is coupled to flow along a karst fracture or conduit, then the combination of this characteristic time scale with the flow velocity leads to a characteristic length scale (Covington et al., 2012). These length scales provide a quantitative tool for dividing different dynamic regimes, and for estimating the decay of critical zone processes with depth.

Process length scales are a specific example of dimensional analysis, whereby characteristic length scales, time scales, and relevant dimensionless numbers are derived from the equations governing a process. Here, I summarize previous use of such methods to understand processes relevant to karst CZ dynamics and then use this framework to generate questions and hypotheses concerning karst CO_2 dynamics and to test assumptions of current models.

DIMENSIONAL ANALYSIS OF PROCESSES IN THE KARST CRITICAL ZONE

Heat Transport

Temperature is an important control on many of the chemical reactions that drive CZ processes, including dissolution and microbial production of CO_2. Temperature variations at Earth's surface propagate into the soil and rock and penetrate to a depth that is often referred to as the thermal penetration depth, or skin depth (Incropera et al., 2007, pg. 299). This depth is dependent on the time scale of temperature variations and is given by a relationship of the form

$$\lambda_{skin} \sim \sqrt{D_{th} t}, \quad (1)$$

where D_{th} is the thermal diffusivity of rock, and t is the timescale of temperature variations. Fluxes of air and water may enhance the depth of surface influence on soil and rock temperatures within the subsurface. Specifically, karst conduits provide pathways that exchange both air and water with the surface. Luetscher and Jeannin (2004) found that flow of both of these fluids can result in substantial heat exchange within a karst system, and that air temperature with depth in a karst aquifer normally trends with the adiabatic lapse rate, demonstrating the importance of air circulation. Wigley and Brown (1971) derived characteristic length scales associated with equilibration of atmospheric air to cave conditions. Using equations for the exchange of heat between fluid and rock, one can derive the thermal length scale associated with fluid flow down a fracture or conduit within the subsurface (Covington et al. 2012). All of these relationships allow relatively simple calculations of the depth to which thermal variations should penetrate into the karst CZ under different conditions. Roughly speaking, conductive heat changes penetrate a few meters into the subsurface, air temperature changes penetrate a few hundreds of meters, and water temperature changes can penetrate pathways multiple kilometers in length, though relatively large (meter scale) conduits are needed for air and water temperature changes to reach such distances into the subsurface.

Dissolution

The most widely discussed length scale in karst is the dissolutional penetration length (Weyl, 1958; Dreybrodt, 1990; Palmer, 1991), the distance that undersaturated water will penetrate along a flow path before approaching saturation. Within a linear kinetic regime, and at a constant flow velocity, water will approach saturation exponentially over a length scale

$$\lambda_d = \frac{V D_H}{4\alpha_s}, \quad (2)$$

where V is the flow velocity, D_H is the hydraulic diameter of the flow path, and α_s is the linear kinetic rate constant (for a derivation see Covington et al., 2012). However, calcite dissolution kinetics become non-linear as saturation is approached, allowing slightly undersaturated water to penetrate much deeper than it would otherwise (Dreybrodt, 1990; Palmer, 1991). Consideration of the exponential length scale in Equation 2 allows an approximation of the distance over which most of the aggressivity of the water is spent. Gabrovšek (2007; 2009) examined the vertical distribution of dissolution rates as water percolates through the vadose zone. This analysis was used to explore the relationship between measured solute fluxes and surface denudation rates within a karst basin. Dissolution length scales have also been compared against CO_2 degassing length scales and matrix inflow length scales to aid interpretation of observed downstream decreases of dissolution rates in a cave stream (Covington et al., 2013). In general, dissolution length scales are quite long (tens to hundreds of km) in mature karst conduits (Covington et al., 2012), so changes in dissolution rates along a conduit are more likely to be a function of CO_2 dynamics or mixing of waters with different chemistries than dissolution occurring along the flow path.

Carbon Dioxide Dynamics

Carbon dioxide, as the primary source of aggressivity in karst waters, provides an important control on the distribution and rate of weathering processes within the karst Critical Zone. CO_2 is produced within the soil zone due to root respiration and oxidation of organic material. However, data from a number of sites also demonstrate that CO_2 concentrations can increase with depth to values much higher than found in the soil zone, suggesting the presence of deeper sources of CO_2 in some settings, likely as the result of organic matter decay deeper within the vadose zone or at the water table (Atkinson, 1977; Wood and Petraitis, 1984; Baldini et al., 2006; Whitaker and Smart, 2007a; Benavente et al., 2010). Models of vadose zone CO_2 profiles within karst are typically based on diffusive transport equations (e.g. Wood, 1985; Breecker et al., 2012), that assume that molecular diffusion is the primary mechanism for transport of CO_2 produced in the subsurface. Diffusive flux is described by Fick's 1st Law, which at steady state gives

$$F_{CO2} = \frac{D_a}{L}[(\mathrm{CO_2})_L - (\mathrm{CO_2})_0], \quad (3)$$

where F_{CO2} is the flux of CO_2, D_a is the diffusion coefficient of CO_2 in air, L is the depth of the CO_2 source, and $(CO2)_L$ and $(CO2)_0$ are the concentrations of CO_2 at depth L and the surface, respectively. An attractive feature of diffusive models is that they can explain relatively high CO_2 concentrations at depth. At equilibrium, the flux of CO_2 out of the vadose zone must be equal to the production rate within it. Therefore, even a modest production of CO_2 at depth will result in an increase in CO_2 concentration at depth until a sufficient gradient is obtained to sustain the required flux (Wood and Petraitis, 1984). However, the dissolutionally enlarged pathways within a karst setting can allow for advective transport of species in both the liquid and gaseous phases. A number of authors have noted that cave ventilation can be an important control on CO_2 within a cave, and consequently on the timing and magnitude of calcite precipitation on speleothems (Spötl et al., 2005; Wong et al., 2011; Frisia et al., 2011; Breecker et al., 2012; Fairchild and Baker, 2012). However, less consideration has been given to whether advective processes influence CO_2 dynamics within smaller aperture flow paths, such as solutionally enlarged fractures. Below, I use dimensional analysis of simple mathematical models of these processes to examine the potential influence of advection.

Advection of gaseous CO2

Since transport of CO_2 in the gas phase through the vadose zone is typically assumed to be diffusive, yet karst vadose zones contain relatively open pathways that may allow advection to occur, I will first examine the conditions under which one might expect for advection of gases along fractures to be important. A number of mechanisms can drive cave airflow, although arguably the most important type of cave airflow is chimney-effect airflow (Wigley and Brown, 1976), whereby temperature-related contrasts between surface and subsurface air density drive buoyant flow between two or more entrances at different elevations. While this airflow mechanism is well-documented within human-enterable caves, an interesting question is whether it might drive significant flow within the fracture systems as well. The pressure difference, ΔP, that drives chimney effect airflow can be approximated as

$$\Delta P = \rho_{in} g h \frac{\Delta T}{T_{ext}}, \quad (4)$$

where ρ_{in} is the density of air inside the cave or fracture, g is Earth's gravitational acceleration, h is the elevation difference between the two openings to the surface, ΔT is the temperature difference between the subsurface and surface air, and T_{ext} is the surface air temperature in Kelvin (e.g. Badino, 2010). Considering laminar flow within a fracture, the flow velocity is given by the Hagen-Pouseuille equation,

$$V = \frac{\Delta P\, a^2}{12\, \mu_a\, L}, \quad (5)$$

Where V is the flow velocity, a is the fracture aperture, μ_a is the dynamic viscosity of air, and L is the length of the flow path. For turbulent flow conditions, the flow velocity is given by the Darcy-Weisbach equation

$$V = \sqrt{\frac{4a\Delta P}{fL}}, \quad (6)$$

where f is the Darcy-Weisbach friction factor. The Peclet Number (Pe), which is the ratio of diffusive and advective time scales, is used to quantify the relative importance of diffusion and advection,

$$\mathrm{Pe} = \frac{VL}{D}, \quad (7)$$

where D is the diffusion coefficient for the species of interest and L is the length scale of interest, which is chosen here to be equal to the flow path length (Incropera et al., 2007). When $\mathrm{Pe} \gtrsim 1$ advective transport is important, and when $\mathrm{Pe} \gg 1$ then transport is dominated by advection rather than diffusion (Fetter, 1993). Note that, unless flow velocity is zero, there will always exist a length scale, L, above which advection is dominant. For laminar flow, Equations 4, 5, and 7 can be combined to give

$$\mathrm{Pe}_{\mathrm{a,lam}} = \frac{\rho_{in} g h a^2}{12\, \mu_a\, D_a} \frac{\Delta T}{T_{ext}}. \quad (8)$$

If one uses the flow path length, L, as the characteristic scale for which Pe is calculated, then for the laminar flow case Pe is independent of flow path length. For turbulent flow, Equations 4, 6, and 7 are combined giving

$$\mathrm{Pe}_{\mathrm{a,turb}} = \frac{L^{1/2}}{D_a} \sqrt{\frac{4\rho_{in} g h a}{f} \frac{\Delta T}{T_{ext}}}. \quad (9)$$

For turbulent flow, Pe does depend on flow path length, and therefore calculation of Pe requires more information about the geometry of the flow path than in the laminar case.

To quantify the potential importance of advective processes within fractures in the karst vadose zone, I calculate Pe for a range of fracture apertures, a, and for entrance elevation differences of 0.3, 3, 30, and 300 m (Figure 1). A temperature ratio (in Kelvin) of $\Delta T / T_{ext} =$ 3.5% is assumed, which corresponds roughly to a difference between surface and subsurface temperatures of 10˚C with a subsurface temperature of 10˚C. This choice is well within the expected range for natural systems. Air properties are also taken at 10˚C with $\rho_{in} = 1.25$ kg m^{-3}, $\mu_a = 1.8 \times 10^{-5}$ (N·s) m^{-2}, and $D_a = 1.55 \times 10^{-5}$ m^{2}s^{-1}. For turbulent flow cases, a value of $f = 0.1$ is used, though the conclusions do not depend strongly on this choice since all of the turbulent flow cases are well within the advective regime. For turbulent flow, the flow path length influences Pe, and therefore two example cases are chosen. In the first case (Figure 1A,B), L is set equal to the difference between the two entrance elevations, h. This is a limiting case, as L cannot be any shorter. However, it provides a reasonable approximation to a vertical fracture that intersects a horizontal cave (Figure 1A). For the second case L=100 h, which represents a situation where the flow path length is much greater than the elevation difference between the two fracture outlets (Figure 1C,D).

Figure 1 suggests that advection should be important in a wide variety of cases. For example, even with a small elevation difference of 0.3 m, advection is an important process within fractures with apertures on the order of 0.1 mm and larger. Differences between the short (Figure 1A,B) and long flowpath (Figure 1C,D) cases are relatively minor because of: 1) the independence of the laminar Pe on flow path length, and 2) the weak dependence of Pe on flow path length in the turbulent regime. For the long flow path case, the transition to turbulence occurs at slightly larger apertures and Pe, and the turbulent flow Pe values are also a factor of 10 larger. This results because of the positive effect of length on Pe that is only partially offset by additional flow resistance.

The above analysis considers fractures that are open to the surface. While exposed fractures are likely to occur in many karst settings, often the rock will be covered by a layer of soil or regolith. Such a cover can substantially influence the extent of air exchange through the fracture network below. If the cover behaves as a porous medium, then the specific discharge of air through the cover is given by Darcy's Law,

$$q = \frac{\kappa \Delta P_p}{\mu_a L_p}, \quad (10)$$

where q is the specific discharge, κ is the permeability, ΔP_p is the pressure drop across the porous cover, and L_p is the thickness of the cover. If the porous cover and fracture are connected in series, then one can assume that the flow velocity in the fracture is equal to the specific discharge in the cover and that the total chimney effect pressure drop (Equation 4) is equal to the sum of the pressure drops across the cover and fracture. Using these assumptions, assuming laminar flow, and again setting the characteristic length scale to the fracture flow path length, leads to a new relation for Pe inside the fracture in the case of cover,

$$\mathrm{Pe}_{\mathrm{a,cover}} = \frac{\rho_{in} g h}{\mu_a D_a} \frac{\Delta T}{T_{ext}} \left(\frac{1}{12/a^2 + F/\kappa} \right), \quad (11)$$

where F is the ratio of cover thickness to fracture length. There are two limiting cases for $\mathrm{Pe}_{\mathrm{a,cover}}$. When $\frac{12}{a^2} \gg \frac{F}{\kappa}$, then the bulk of the pressure loss is in the fracture, the cover has little effect, and Equation 8 applies. Alternatively, when $\frac{12}{a^2} \ll \frac{F}{\kappa}$, then the bulk of the pressure loss is in the cover, and the fracture properties no longer influence Pe. Comparing the magnitude of these two terms allows estimation of the strength of the influence of the cover. In the limit where the pressure loss is entirely in the cover, Pe approaches a maximum possible value of

$$\mathrm{Pe}_{\mathrm{a,max}} = \frac{\kappa \rho_{in} g h}{\mu_a D_a F} \frac{\Delta T}{T_{ext}}. \quad (12)$$

Two example cases are shown in Figure 2, where F=0.05 and κ is set to 10^{-9} m^2 in the first case (Figure 2A) and 10^{-12} m^2 in the second (Figure 2B). One can see that there are realistic cases where the cover would either allow advection to dominate or would shut it down. This model likely produces an underestimate of the importance of advection, since it assumes that the air exiting or entering the fracture will pass through a column of cover equal in cross sectional area to the fracture. More likely, air would spread through a cone within the cover and perhaps channel along preferential flow paths due to heterogeneity within the cover.

Advection of water and its influence on CO2

In the previous section I examined whether advection within the gaseous phase may play an important role in the karst vadose zone. However, even in the absence of gas advection along fractures and conduits, water is channeled along these flow paths, particularly during wet periods or following recharge events. The water and air do not evolve in isolation but rather CO_2 will exchange between the two. Here I will examine whether advective flows of water can influence an otherwise diffusive CO_2 profile within a fracture. To examine this question, I use coupled advection-dispersion equations for air and water within a fracture,

$$\frac{\partial(\mathrm{CO_2})_w}{\partial t} = D_w \frac{\partial^2(\mathrm{CO_2})_w}{\partial x^2} - V_w \frac{\partial(\mathrm{CO_2})_w}{\partial x} - \frac{D_w}{\delta_w^2}\left[(\mathrm{CO_2})_w - \alpha(\mathrm{CO_2})_a\right] + R, \quad (13)$$

$$\frac{\partial(\mathrm{CO_2})_a}{\partial t} = D_a \frac{\partial^2(\mathrm{CO_2})_a}{\partial x^2} - V_a \frac{\partial(\mathrm{CO_2})_a}{\partial x} + \frac{D_w}{\delta_w \delta_a}\left[(\mathrm{CO_2})_w - \alpha(\mathrm{CO_2})_a\right], \quad (14)$$

where t is time, x is position along the fracture, $(CO_2)_a$ and $(CO_2)_w$ are CO_2 concentrations in the air and water, respectively, D_w is the diffusion coefficient for CO_2 in water, V_w and V_a are the flow velocities of air and water, respectively, δ_w is the thickness of the water film on the fracture wall, δ_a is the aperture of the air-filled portion of the fracture, α is the Ostwald solubility coefficient for CO_2 (Wanninkhof et al., 2009), and R is a term representing CO_2 production within the water or at the water-rock boundary. The geometry of this model is depicted in Figure 3. The exchange terms (the third terms on the right hand side of each equation) assume that CO_2 exchange is controlled by the rate of diffusion of CO_2 through the water film. This simple model is arguably a gross oversimplification of dynamics in karst fractures, but dimensional analysis of the model will allow an initial examination of assumptions and elucidation of relevant process controls. One process not represented in Equations 13 and 14 is the interaction between CO_2 concentrations and dissolution or precipitation of calcite. These processes are discussed briefly below, and can easily be introduced with an additional term, but are excluded here for the sake of brevity.

To examine whether flowing water might influence CO_2 profiles within the vadose zone, I consider a case where air velocity is zero, such that the CO_2 profile, if unperturbed by the flow of water, would be controlled by diffusion. Setting the time derivative terms to zero allows us to examine steady state CO_2 profiles, and for simplicity I also consider a case with no CO_2 production (*R*=0*)*. To non-dimensionalize the model, I define a dimensionless position variable $x^* = x/L$, and dimensionless concentration, $(CO_2^*)_i=(CO_2)_i/(CO_2)_0$, where L is a characteristic length scale, and $(CO_2)_0$ is a reference concentration of CO_2. In the example solutions below, $(CO_2)_0$ is set to the standard atmospheric concentration of CO_2, though any reference value could be used. Using these definitions and assumptions, Equations 13 and 14 can be re-written as

$$\frac{1}{\mathrm{Pe}_w}\frac{\partial^2(\mathrm{CO}_2^*)_w}{\partial x^{*2}} = \frac{\partial(\mathrm{CO}_2^*)_w}{\partial x^*} + \Lambda_w[(\mathrm{CO}_2^*)_w - \alpha(\mathrm{CO}_2^*)_a], \quad (15)$$

$$\frac{\partial^2(\mathrm{CO}_2^*)_a}{\partial x^{*2}} = -\xi[(\mathrm{CO}_2^*)_w - \alpha(\mathrm{CO}_2^*)_a], \quad (16)$$

where $\mathrm{Pe_w} = V_w L/D_w$, $\xi = D_w L^2/D_a\delta_w\delta_a$, and $\Lambda_w = D_w L/\delta_w^2 V_w$ are all dimensionless numbers that determine the nature of the solution. $\mathrm{Pe_w}$ is the Peclet Number for transport within the water and determines the relative importance of advection and diffusion along the flowing film. $\xi = (D_w L/\delta_w)/(D_a\delta_a/L)$ represents the ratio between the water-air CO_2 exchange rate and the diffusive mass transport rate within the air along the length of the fracture. When ξ is large, then exchange of CO_2 between the water and air will be important in comparison to diffusion in the air along the fracture. When ξ is small then exchange is insignificant in comparison to diffusive transport. The final dimensionless number, $\Lambda_w = L/\lambda_w$, is a ratio of the fracture length and the length scale over which the water CO_2 concentration equilibrates with the air, $\lambda_w = V_w \delta_w^2 / D_w$. If Λ_w is small, then the water CO_2 concentration will be decoupled from the air. If Λ_w is large, then the CO_2 concentration in the water will remain nearly equilibrated to that of the air over length scales greater than L. These dimensionless numbers are summarized in Table 1.

(Table 1 near here)

In order for flow of water through the vadose zone to influence CO_2 profiles within the air, two physical conditions must hold: 1) the rate of transfer of CO_2 between air and water must be comparable to or greater than the rate of diffusive transport within the air, otherwise any perturbations to the profile via exchange will be efficiently smoothed by diffusion in the air, and 2) the advective mass transport rate of CO_2 in the water film must be comparable to or greater than the diffusive mass transport rate in the air, otherwise the water will not have the transport capacity to influence CO_2 concentrations in the air. The first condition can be quantified as $\xi \gtrsim 1$. The second condition is met when the ratio $\xi / \Lambda_w = \delta_w V_w / (\frac{D_a \delta_a}{L}) \gtrsim 1$, as this ratio expresses the ratio of the mass transport rate via advection in the water to the mass transport rate via diffusion in the air. For $\xi / \Lambda_w < 1$ the diffusive transport in the air outpaces advective transport in the water, and the film has no significant affect. This occurs in the limit of low film velocity and thin films.

To determine whether downward flow of water is likely to influence air CO_2 profiles in nature, we can examine typical values of the dimensionless numbers ξ and Λ_w under conditions that occur in natural systems. Concerning ξ, the ratio of the diffusion coefficients for CO_2 in air and water is roughly constant, $D_w / D_a \approx 10^{-4}$. Therefore we need only consider the other variables, L, which can be taken to be the thickness of the vadose zone or the length of the fracture flow path, and δ_a and δ_w, which are the aperture of the air-filled fracture and the thickness of the water film, respectively. For a thin film of water flowing on a vertical wall, the thickness of the film can be approximated as (Bird et al., 2002)

$$\delta_w = \sqrt{\frac{3V_w\mu_w}{g\rho_w}}. \qquad (17)$$

Using this relationship and the ratio of diffusion coefficients above, the equations for ξ and Λ_w can be rewritten in terms of V_w as

$$\xi = \frac{10^{-4}L^2}{\delta_a}\sqrt{\frac{g\rho_w}{3V_w\mu_w}} \qquad (18)$$

$$\Lambda_w = \frac{LD_w g\rho_w}{3V_w^2\mu_w}. \qquad (19)$$

To examine the likely ranges of these parameters in nature, I calculate ξ and Λ_w for fractures/conduits with air-filled apertures of 0.001 m and 0.1 m and for vadose zone thicknesses of L = 0.3, 3, 30, and 300 m. The dimensionless parameters are calculated as a function of V_w over a range from 10^{-6} m s^{-1} to 10 m s^{-1} (Figure 4). ξ is small for only a few cases where the vadose zone is very thin and the flow very fast. Therefore the ratio ξ/Λ_w, which expresses the relative rates of mass transport in the water and air, is the primary determining factor for whether the water influences the air CO_2 profile. The water advective influence is stronger for thicker vadose zones and when the air-filled aperture is smaller (Figure 4A). However, in most settings air CO_2 profiles are influenced by water advection for flow velocities above about 1 mm s^{-1}, which is well within the range of expected velocities in natural fractures.

To illustrate the influence of these dimensionless numbers on the shape of equilibrium CO_2 profiles, and the likely importance of advection, I numerically solve Equations 15 and 16 in Python using the free and open source finite volume package FiPy (Guyer et al., 2009). The equations are solved at steady-state for the boundary conditions

$$\frac{1}{\alpha}(\mathrm{CO}_2^*)_w|_{x=0} = (\mathrm{CO}_2^*)_a|_{x=0} = 1, \qquad (20)$$

$$(\mathrm{CO}_2^*)_a|_{x=L} = 10 \quad (21)$$

$$\frac{d(\mathrm{CO}_2^*)_w}{dx}|_{x=L} = 0. \quad (22)$$

The first two boundary conditions (20) set the air and water CO_2 at the top of the fracture to values that are equilibrated with the atmosphere. The third condition (21) sets the CO_2 concentration at depth L equal to 10 times atmospheric, and the final condition (22) is an outlet boundary condition at the downstream end of the water film. These boundary conditions represent the case of a CO_2 source at depth L, which is only one of many possibilities. For example, profiles would look quite different for a source near the surface. However, solutions for this example set of boundary conditions will illustrate how the dimensionless parameters, and the relative importance of physical processes that they represent, influence the form of the solution. These conclusions also hold for other conditions, such as a near-surface CO_2 source, although the shapes of the profiles will, in general, be different.

Solutions are shown for four example cases that span a variety of possible combinations of the dimensionless parameters. Individual profiles are shown in Figure 5 and their location on Figure 4 is also marked with identifying numbers. When ξ is small, the water film has no significant influence on the air CO_2, and the profile closely matches that of the purely diffusive case (Figure 5A). If $\xi > 1$ and $\Lambda_w < 1$ then the CO_2 air profile is strongly influenced by the water, but the water film CO_2 concentration is not strongly affected by the air CO_2 as the water film is moving too quickly to be significantly influenced (Figure 5B). When both ξ and Λ_w are significantly larger than one and $\xi/\Lambda_w \gtrsim 1$, then the air CO_2 profile is significantly influenced by the water film, but the water film stays near equilibrium with the air at all depths (Figure 5C). Finally, when $\xi \gg 1$ and $\xi/\Lambda_w \lesssim 1$ then the CO_2 profile is nearly diffusive and the water profile is close to equilibrium with the air, because the water film has insufficient transport capacity in comparison to diffusion rates in the air (Figure 5D).

DISCUSSION AND CONCLUSIONS

While the models presented here are simple, and natural karst systems undoubtedly display a broader and richer range of dynamics, these simple models provide an initial means of thinking about the relative importance of different processes and the likely interactions between them. In the past, vadose zone gas dynamics has typically been treated as diffusive, where advective transport, within both the gas and liquid phases, is neglected (Penman, 1940a; Penman, 1940b; Marshall, 1959; Wood and Petraitis, 1984). Buoyancy driven flows have received recent consideration within fracture systems (Weisbrod and Dragila, 2006; Weisbrod et al., 2009; Nachshon et al., 2008). However, in karst systems dissolutional enlargement of fractures may further increase the importance of advective processes.

In the models presented above, I first examine the possibility of advective air flows that are driven by chimney effect pressure gradients. The influence of cave air flow patterns on CO_2 concentrations has been well-documented (Troester and White, 1984; Ek and Gewelt, 1985; Spötl et al., 2005; Baldini et al., 2008; Milanolo and Gabrovšek, 2009; Wong et al., 2011; Breecker et al., 2012; Gulley et al., 2014), and chimney effect airflow is arguably the most common mechanism of cave airflow (Wigley and Brown, 1976). Previous authors have demonstrated, using similar dimensional analysis, that advection should be a dominant process for CO_2 transport in human-enterable caves (Frisia et al., 2011; Fairchild and Baker, 2012). However, the dimensional analysis above suggests that chimney effect airflow should also be important in many fractures or small solutionally enlarged pathways. For example, a fracture with a 1 mm aperture that has two entrances with an elevation difference of only 0.3 m has a

Peclet Number of more than 100 in the case of a surface temperature 10 degrees different from the subsurface temperature. This indicates that transport should be predominantly advective in that case. Advection becomes even stronger with larger elevation differences. The suggested importance of advection through smaller diameter flow paths is consistent with field data. For example, Obir Cave, with no known upper entrance, displays strong chimney effect airflow (Spötl et al., 2005).

Since fractures that are open to the surface should experience significant airflow in a wide variety of conditions (Figure 1), the presence of significant chimney effect air flow is likely to be primarily a function of cover. If there is a thick, relatively impermeable, cover then this will shut down chimney effect airflow within the fracture network below it. The extent to which a cover impedes airflow can be approximated by calculating the theoretical maximum Peclet Number (Equation 12) appropriate for the cover thickness and permeability, though this approach is likely to somewhat overestimate the capability of the cover to halt air circulation. The fracture network pattern, and particularly the extent of horizontal connectivity, is also likely to be an important control. A fracture network with more extensive horizontal connectivity is more likely to host connected pathways that intersect the surface at substantially different elevations.

Even if advection dominates CO_2 transport within fractures and caves, one might ask whether this influence exists only in isolated zones in the vicinity of these preferential flow paths. It may be the case that some portions of the vadose zone are isolated from the effects of advection. However, diffusion occurs both vertically and laterally. Therefore the influence of advection at a particular point within the vadose zone is likely to depend on the ratio of the distance between that point and the surface and that point and the nearest advection-dominated path (Figure 6). If, at a given location, the nearest advection-dominated path is closer than the surface, then advection is likely to have an important influence at that location. Of course, any anisotropy between vertical and lateral diffusion rates must also be accounted for.

Chimney effect airflow implies that there are regions of both inflow and outflow of air that vary with season and surface temperature. Therefore, CO_2 dynamics can be expected to vary diurnally and seasonally. Lower and upper entrances will also experience substantially different CO_2 dynamics and gradients with depth, since each undergoes the opposite direction of flow at any given time. Such effects may have important implications for the temporal and spatial distribution of geomorphic work within the karst vadose zone. In comparison to chimney effect airflow, karst systems dominated by barometric air exchange would be expected to display quite different distributions of CO_2 in space and time.

The model presented for the coupling between water and air CO_2 concentrations suggests that flowing water, even in the absence of air flow, is likely to alter CO_2 profiles away from purely diffusive profiles to curved profiles that display lower gradients near the surface and higher gradients at depth. The exact shape will depend on the boundary conditions at the water table and the distribution of CO_2 production with depth. In particular, the example cases shown in Figure 5 assume CO_2 production is located at depth. Different distributions of CO_2 production can result in quite different vertical CO_2 profiles than the ones depicted here. The strength of the advective influence of water depends on several parameters, but, for most of the parameter space sampled, water flow velocities of 1 mm s^{-1} and greater typically result in a CO_2 profile that is modified by water advection. Within natural systems, such effects are likely to be event driven, and the profile may evolve seasonally and with individual recharge events. The ability for a diffusive profile to recover between recharge events will be largely dependent on the ratio of the diffusion time scale for the vadose zone thickness to the time period between recharge events that modify the profile.

There are a variety of processes that are not considered explicitly here, but for which a similar approach may enable fruitful progress. One might ask whether there are typical length scales that govern CO_2 production within the subsurface. For example, roots may penetrate to typical depths that vary by plant species and other parameters. Filtration and processing of particulate and dissolved organic matter may also have associated length scales that depend upon rates of microbial decay, soil porosity and permeability, fracture aperture, recharge rate, and temperature. Understanding these controls will substantially improve our ability to predict the distribution of CO_2 within karst Critical Zones in different settings. Any length scales associated with CO_2 production could be compared against length scales of water-air CO_2 exchange to quantify the influence that production would have on the overall profile.

Similarly, comparing dissolutional length scales with CO_2 exchange and production length scales would improve our understanding of the distribution of geomorphic work throughout the karst Critical Zone. Under what conditions is aggressivity largely spent near the zone where it is produced versus penetrating much greater depths before the CO_2 has reacted? In cases where dissolutional length scales are much shorter than CO_2 exchange length scales then dissolution and/or precipitation is also likely itself to be an important driver of CO_2 dynamics. Similar coupling between wind-driven ventilation and dissolution/precipitation has been observed within a semi-arid karst setting (Roland et al., 2013).

The analysis presented here, motivated from a physics-based approach, is entirely theoretical. One might ask what implications it has for field studies of CO_2 dynamics in karst. I would argue that there are several important implications. First, while prior models have typically assumed CO_2 transport in the vadose zone is diffusive, relatively simple models of buoyancy driven flow and transport within the karst vadose zone suggest that typical conditions can produce advective effects driven by flow of air or water. Therefore, interpretation of vadose zone CO_2 dynamics in karst should not assume from the start that diffusion is dominant and that flow of water does not perturb CO_2 concentrations. The model presented here also provides a mathematical starting point for quantifying advective effects and understanding the influence they may have on CO_2 distributions in time and space. CO_2 profiles under the influence of advection are more likely to contain sharp features that correlate with different air or water circulation zones and to change dynamically with changes in surface temperature and recharge rate. Such effects have been observed within a deep karst vadose zone in Spain within boreholes where air flow was also observed (Benavente et al., 2010).

Spatial and temporal variability in CO_2 may also play an important an important role in speleogenesis (Gabrovšek and Dreybrodt, 2000; Gabrovšek et al., 2000; Whitaker and Smart, 2007b; Gulley et al., 2013; Gulley et al., 2014), and advective processes are likely to be an important control on the spatial and temporal distribution of dissolution within mature cave systems. The distribution of CO_2 within the vadose zone, the rate of exchange of CO_2 between air and water, and the interactions between water and rock via dissolution or precipitation all influence carbon isotope fractionation (Fairchild and Baker, 2012, p. 176-180). Therefore, the conclusions here concerning the importance of advection have important implications for studies of paleoclimate that employ speleothems.

In summary, the models presented here suggest that CO_2 dynamics within the karst Critical Zone may be controlled by a number of processes that have traditionally been neglected. Currently, there is little data available to constrain the range of dynamics that occur in natural systems. Data campaigns that sample densely in both space and time may provide substantial insight into the processes that drive landform and subsurface evolution in karst terrains.

Acknowledgments

I appreciate stimulating discussions with Matija Perne and Joe Myre during the development of this model. Insightful comments by reviewers Steffen Birk, Ian Fairchild, and Pierre-Yves Jeannin also helped to substantially clarify and sharpen this work.

Atkinson, T.C., 1977, Carbon dioxide in the atmosphere of the unsaturated zone an important control of groundwater hardness in limestones: Journal of Hydrology, v. 35, no. 1-2, p. 111–123.

Badino, G., 2010, Underground meteorology - “What’s the weather underground?” Podzemna meteorologija: “Kakšno je vreme v podzemlju?:” Acta Carsologica, v. 39, no. 3, p. 427–448.

Baldini, J.U.L., Baldini, L.M., McDermott, F., and Clipson, N., 2006, Carbon dioxide sources, sinks, and spatial variability in shallow temperate zone caves: evidence from Ballynamintra Cave, Ireland.: Journal of Cave and Karst Studies, v. 68, no. 1, p. 4–11.

Baldini, J.U.L., McDermott, F., Hoffmann, D.L., Richards, D. a., and Clipson, N., 2008, Very high-frequency and seasonal cave atmosphere PCO2 variability: Implications for stalagmite growth and oxygen isotope-based paleoclimate records: Earth and Planetary Science Letters, v. 272, no. 1-2, p. 118–129, doi: 10.1016/j.epsl.2008.04.031.

Benavente, J., Vadillo, I., Carrasco, F., Soler, A., and Moral, F., 2010, Air Carbon Dioxide Contents in the Vadose Zone of a Mediterranean Karst: v. 9, no. 1, p. 126–136, doi: 10.2136/vzj2009.0027.

Bird, R.B., Stewart, W.E., and Lightfoot, E.N., 2002, Transport phenomena: John Wiley and Sons, New York.

Brantley, S.L., White, T.S., White, A.F., Sparks, D., Richter, D., Pregitzer, K., Derry, L., Chorover, J., Chadwick, O., April, R., Anderson, S., and Amundson, R., 2006, Frontiers in Exploration of the Critical Zone: A report of the workshop sponsored by the National Science Foundation (NSF), October 24-26, 2005:, 30p. p.

Breecker, D.O., Payne, A.E., Quade, J., Banner, J.L., Ball, C.E., Meyer, K.W., and Cowan, B.D., 2012, The sources and sinks of CO2 in caves under mixed woodland and grassland vegetation: Geochimica et Cosmochimica Acta, v. 96, p. 230–246, doi: 10.1016/j.gca.2012.08.023.

Covington, M.D., Luhmann, A.J., Wicks, C.M., and Saar, M.O., 2012, Process length scales and longitudinal damping in karst conduits: Journal of Geophysical Research, v. 117, no. F1, p. 1–19, doi: 10.1029/2011JF002212.

Covington, M.D., Prelovšek, M., and Gabrovšek, F., 2013, Influence of CO2 dynamics on the longitudinal variation of incision rates in soluble bedrock channels: Feedback mechanisms: Geomorphology, v. 186, p. 85–95, doi: 10.1016/j.geomorph.2012.12.025.

Dreybrodt, W., 1990, The role of dissolution kinetics in the development of karst aquifers in limestone: a model simulation of karst evolution: Journal of Geology, v. 98, no. 5, p. 639–655.

Ek, C., and Gewelt, M., 1985, Carbon dioxide in cave atmospheres. New results in Belgium and comparison with some other countries: Earth Surface Processes and Landforms, v. 10, p. 173–187.

Fairchild, I.J., and Baker, A., 2012, Speleothem Science: From Processes to Past Environments: Wiley-Blackwell, West Sussex, UK.

Fetter, C.W., 1993, Contaminant hydrogeology: Macmillian, New York.

Ford, D.C., and Williams, P., 2007, Karst Hydrogeology and Geomorphology: John Wiley and Sons, Chichester, West Sussex, England.

Frisia, S., Fairchild, I.J., Fohlmeister, J., Miorandi, R., Spo, C., and Borsato, A., 2011, Carbon mass-balance modelling and carbon isotope exchange processes in dynamic caves: Geochimica Cosmochimica Acta, v. 75, p. 380–400, doi: 10.1016/j.gca.2010.10.021.

Gabrov\v{s}ek, F., and Dreybrodt, W., 2000, Role of mixing corrosion in calcite-aggressive H2O-CO2-CaCO3 solutions in the early evolution of karst aquifers in limestone: Water Resources Research, v. 36, no. 5, p. 1179–1188.

Gabrov\v{s}ek, F., Menne, B., and Dreybrodt, W., 2000, A model of early evolution of karst conduits affected by subterranean CO2 sources: Environmental Geology, v. 39, no. 6, p. 531–543.

Gabrovšek, F., 2009, On concepts and methods for the estimation of dissolutional denudation rates in karst areas: Geomorphology, v. 106, no. 1-2, p. 9–14, doi: 10.1016/j.geomorph.2008.09.008.

Gabrovšek, F., 2007, On denudation rates in karst: O hitrosti denudacije na Krasu, *in* Time in Karst, Postojna, p. 7–13.

Gulley, J., Martin, J., and Moore, P., 2014, Vadose CO 2 gas drives dissolution at water tables in eogenetic karst aquifers more than mixing dissolution: , doi: 10.1002/esp.3571.

Gulley, J.D., Martin, J.B., Moore, P.J., and Murphy, J., 2013, Formation of phreatic caves in an eogenetic karst aquifer by CO 2 enrichment at lower water tables and subsequent flooding by sea level rise: v. 1224, no. January, p. 1210–1224, doi: 10.1002/esp.3358.

Guyer, J.E., Wheeler, D., and Warren, J.A., 2009, FiPy: Partial differential equations with python: Computing in Science and Engineering, v. 11, p. 6–15, doi: 10.1109/MCSE.2009.52.

Incropera, F.P., Dewitt, D.P., Bergman, T.L., and Lavine, A.S., 2007, Fundamentals of Heat and Mass Transfer: John Wiley and Sons, Hoboken, NJ.

Luetscher, M., and Jeannin, P.-Y., 2004, Temperature distribution in karst systems: the role of air and water fluxes: Terra Nova, v. 16, no. 6, p. 344–350, doi: 10.1111/j.1365-3121.2004.00572.x.

Marshall, T.J., 1959, The diffusion of gases through porous media: Soil Science Society of America Journal, v. 10, no. 1, p. 79–82.

Milanolo, S., and Gabrovšek, F., 2009, Analysis of Carbon Dioxide Variations in the Atmosphere of Srednja Bijambarska Cave, Bosnia and Herzegovina: Boundary-Layer Meteorology, v. 131, no. 3, p. 479–493, doi: 10.1007/s10546-009-9375-5.

Nachshon, U., Weisbrod, N., and Dragila, M., 2008, Quantifying air convection through surface-exposed fractures: A laboratory study: Vadose Zone Journal, v. 7, no. 3, p. 948–956.

Palmer, A.N., 1991, Origin and morphology of limestone caves: Bulletin of the Geological Society of America, v. 103, no. 1, p. 1.

Penman, H.L., 1940a, Gas and vapour movements in the soil: I. The diffusion of vapours through porous solids: Journal of Agricultural Science, v. 30, p. 437–462.

Penman, H.L., 1940b, Gas and vapour movements in the soil: II. The diffusion of carbon dioxide through porous solids: 1Journal of Agricultural Science, v. 30, p. 570–581.

Roland, M., Serrano-Ortiz, P., Kowalski, A.S., Goddéris, Y., Sánchez-Cañete, E.P., Ciais, P., Domingo, F., Cuezva, S., Sanchez-Moral, S., Longdoz, B., Yakir, D., Van Grieken, R., Schott, J., Cardell, C., et al., 2013, Atmospheric turbulence triggers pronounced diel pattern in karst carbonate geochemistry: Biogeosciences, v. 10, no. 7, p. 5009–5017, doi: 10.5194/bg-10-5009-2013.

Sp"{o}tl, C., Fairchild, I.J., and Tooth, A.F., 2005, Cave-air control on dripwater geochemistry, Obir Caves (Austria): Implications for speleothem deposition in dynamically ventilated caves.: Geochimica Cosmochimica Acta, v. 69, p. 2451–2468.

Troester, J., and White, W.B., 1984, Seasonal fluctuations in the carbon dioxide partial pressure in a cave atmosphere: Water Resources Research, v. 20, no. 1, p. 153–156.

Wanninkhof, R., Asher, W.E., Ho, D.T., Sweeney, C., and McGillis, W.R., 2009, Advances in quantifying air-sea gas exchange and environmental forcing: Annual Review of Marine Science, v. 1, no. 1, p. 213–244, doi: 10.1146/annurev.marine.010908.163742.

Weisbrod, N., and Dragila, M., 2006, Potential impact of convective fracture venting on salt-crust buildup and ground-water salinization in arid environments: Journal of Arid Environments, v. 65, p. 386–399.

Weisbrod, N., Dragila, M., Nachshon, U., and Pillersdorf, M., 2009, Falling through the cracks: The role of fractures in Earth-atmosphere gas exchange: Geophysical Research Letters, v. 36, p. L02401.

Weyl, P.K., 1958, The solution kinetics of calcite: The Journal of Geology, v. 66, no. 2, p. 163–176.

Whitaker, F.F., and Smart, P.L., 2007a, Geochemistry of meteoric diagenesis in carbonate islands of the northern Bahamas : 1 . Evidence from field studies: v. 966, no. February, p. 949–966, doi: 10.1002/hyp.

Whitaker, F.F., and Smart, P.L., 2007b, Geochemistry of meteoric diagenesis in carbonate islands of the northern Bahamas : 2 . Geochemical modelling and budgeting of diagenesis: v. 982, no. February, p. 967–982, doi: 10.1002/hyp.

Wigley, T.M.L., and Brown, M.C., 1971, Geophysical applications of heat and mass transfer in turbulent pipe flow: Boundary-Layer Meteorology, v. 1, no. 1968, p. 300–320.

Wigley, T.M.L., and Brown, M.C., 1976, The Physics of Caves, *in* Ford, T.D. and Cullingford, C.H.D. eds., The Science of Speleology, p. 329–358.

Wong, C.I., Banner, J.L., and Musgrove, M., 2011, Seasonal dripwater Mg / Ca and Sr / Ca variations driven by cave ventilation : Implications for and modeling of speleothem paleoclimate records: Geochimica et Cosmochimica Acta, v. 75, no. 12, p. 3514–3529, doi: 10.1016/j.gca.2011.03.025.

Wood, W.W., 1985, Origin of caves and other solution openings in the unsaturated (vadose) zone of carbonate rocks : A model for CO2 generation: Geology, v. 13, p. 822–824.

Wood, W.W., and Petraitis, M.J., 1984, Origin and Distribution of Carbon Dioxide in the Unsaturated Zone of the Southern High Plains of Texas Ca: Water Resources Research, v. 20, no. 9, p. 1193–1208.

Worthington, S.R.H., 2009, Diagnostic hydrogeologic characteristics of a karst aquifer (Kentucky, USA): Hydrogeology Journal, v. 17, no. 7, p. 1665–1678, doi: 10.1007/s10040-009-0489-0.

TABLES

Table 1. Dimensionless numbers that determine the dynamics of the coupled water-air CO_2 transport model.

Dimensionless Number	Physical interpretation
$\mathrm{Pe_w} = V_w L / D_w$	Relative importance of advective and dispersive mass transport within the water film. Advection dominates for large $\mathrm{Pe_w}$.
$\xi = D_w L^2 / D_a \delta_w \delta_a$	Relative importance of mass transfer via water-air exchange and diffusion within the air. Exchange is important for large ξ.
$\Lambda_w = D_w L / \delta_w^2 V_w$	Ratio of fracture length to the length scale associated with CO_2 exchange. For large Λ_w water and air CO_2 are closely coupled.
$\frac{\xi}{\Lambda_w} = L \delta_w V_w / D_a \delta_a$	Relative importance of advective mass transfer in the water and diffusive mass transfer in the air. When this ratio is large mass transfer in the water is important.

Table 2. Description of notation

Symbol	Definition
a	fracture aperture
$\boldsymbol{\alpha}$	Ostwald solubility coefficient
α_s	calcite dissolution kinetic rate constant
(CO_2), $(CO_2)_a$, $(CO_2)_w$	concentration of CO_2, in air, in water
D_a	diffusion coefficient for CO_2 in air
D_w	diffusion coefficient for CO_2 in water
D_H	hydraulic diameter
D_{th}	thermal diffusivity of rock
$\boldsymbol{\delta_a}$	aperture of air-filled portion of fracture
$\boldsymbol{\delta_w}$	thickness of water film on fracture wall
f	Darcy-Weisbach friction factor
F	ratio of cover thickness to fracture length (L_p/L)
$\boldsymbol{F_{CO2}}$	flux rate of CO_2
g	Earth's gravitational acceleration
h	difference in elevation between two entrances
κ	permeability
L	fracture length or characteristic length scale
L_p	thickness of porous cover
Λ_w	$\boldsymbol{D_w L / \delta_w^2 V_w}$, dimensionless number (see Table 1)
λ_d	dissolutional penetration length
λ_w	CO_2 exchange length scale

λ_{skin}	thermal skin depth
μ_a	dynamic viscosity of air
ΔP	pressure difference
ΔP_p	pressure difference across the porous cover
Pe	Peclet Number
ρ_{in}	density of air inside the cave or fracture
q	specific discharge (of air)
R	CO_2 production rate
$\boldsymbol{\Delta T}$	difference in temperature inside and outside cave or fracture
T_{ext}	temperature outside of cave or fracture
t	time
V (V_a or V_w)	velocity (of air or water)
x	position along the fracture
ξ	$\boldsymbol{D_w L^2 / D_a \delta_w \delta_a}$, dimensionless number (see Table 1)

FIGURES

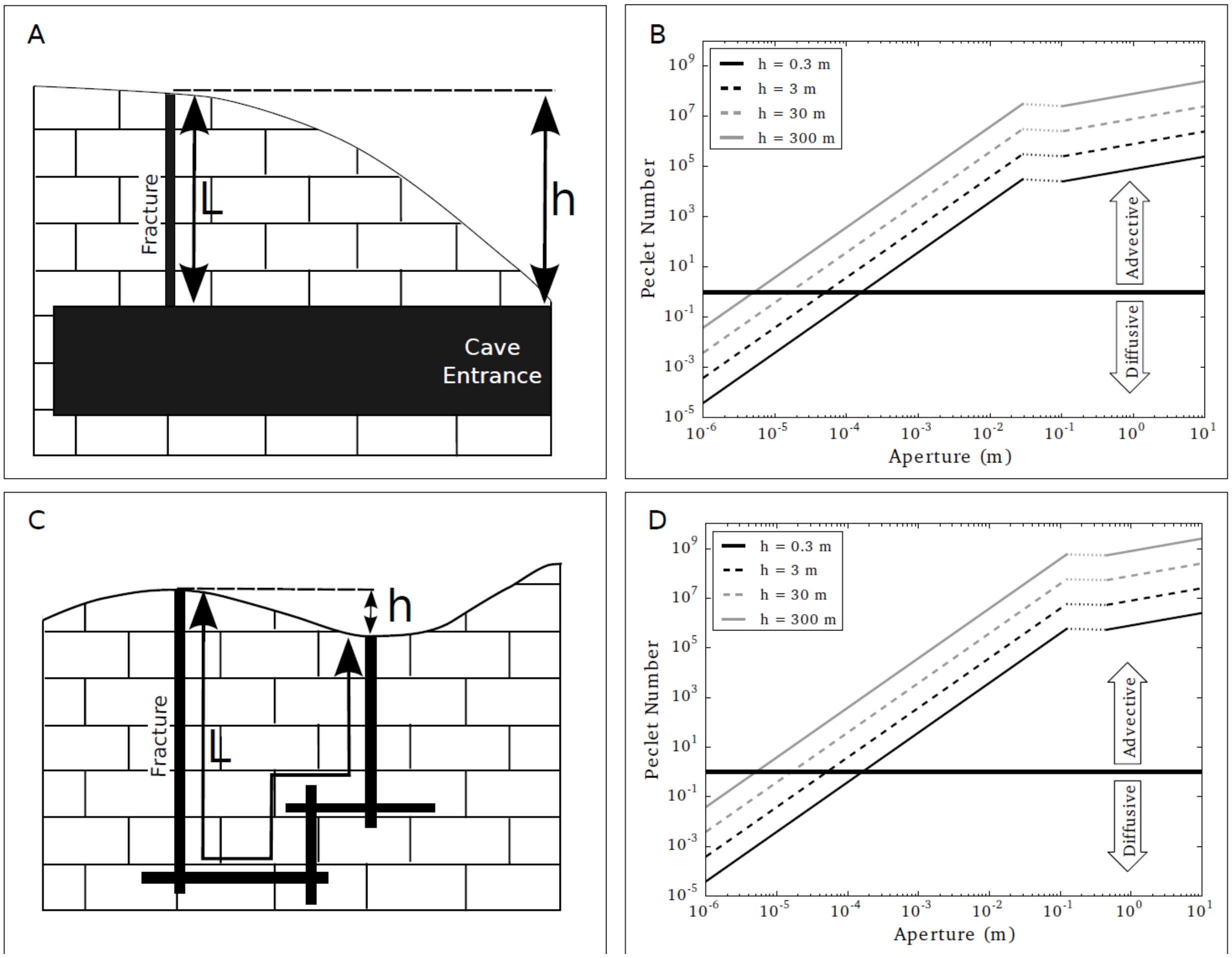

Figure 1. The values of Peclet Number (Pe) for chimney effect airflow in fractures for a range of fracture apertures and differences between entrance elevations (*h*). Transport is dominated by advection for Pe>>1. Panel A shows an example geometry where the fracture length, *L*, is equal to the elevation difference between entrances and Pe is calculated for this case in Panel B. Panel C shows a case where fracture length is much greater than the elevation difference between entrances, and Pe is calculated for $L=100\ h$ in Panel D. Note that this difference has no influence on Pe for the laminar flow regime (i.e. in the left portion of the diagrams). Laminar to turbulent transition occurs within the region with the dotted lines.

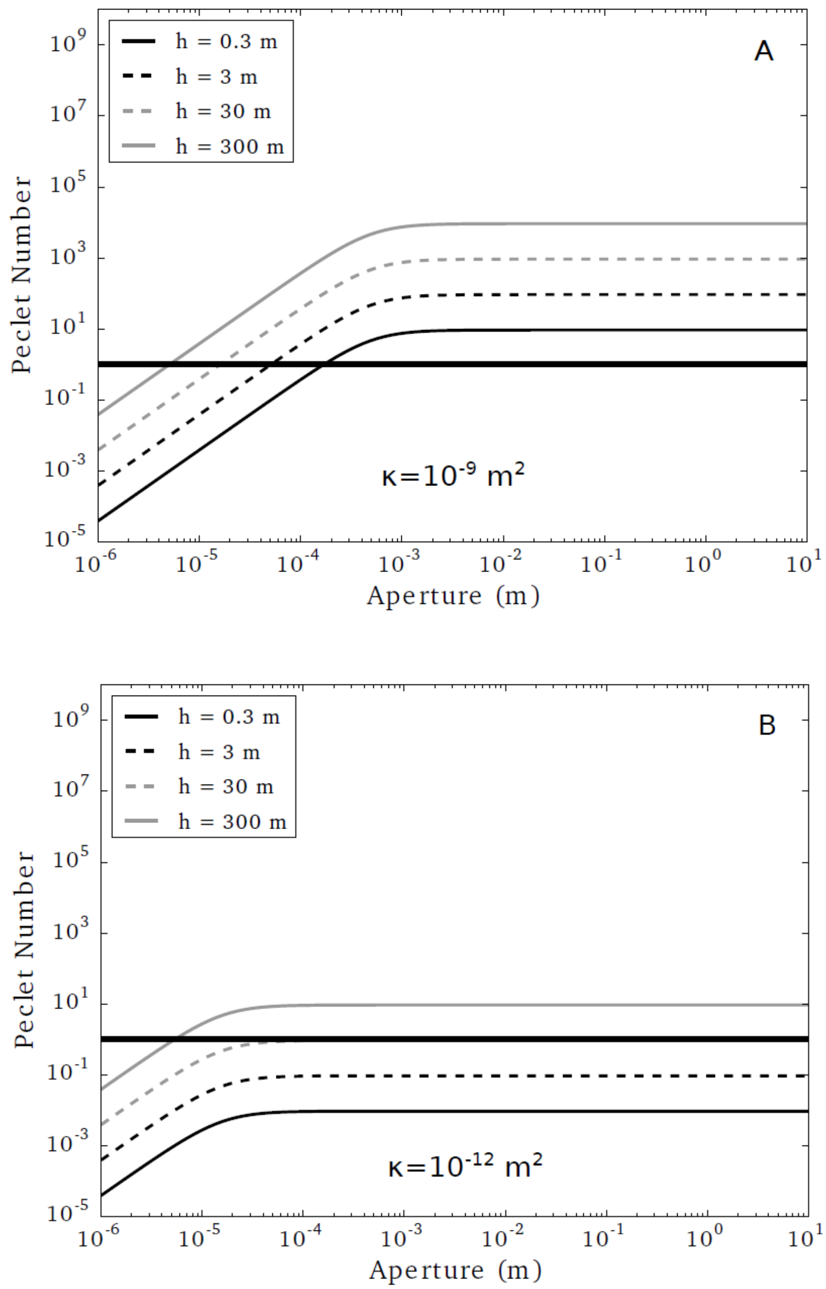

Figure 2. Peclet Numbers (Pe) calculated for chimney effect airflow through fractures with a porous cover. In this case, a maximum value of Pe is reached for a sufficiently large fracture aperture, as all pressure loss occurs in the porous media in that limit. Panel A depicts a case where permeability $\kappa=10^{-9}$ m^2, and Panel B depicts a case where $\kappa=10^{-12}$ m^2. For both cases, the cover thickness is assumed to be 5% of the fracture length.

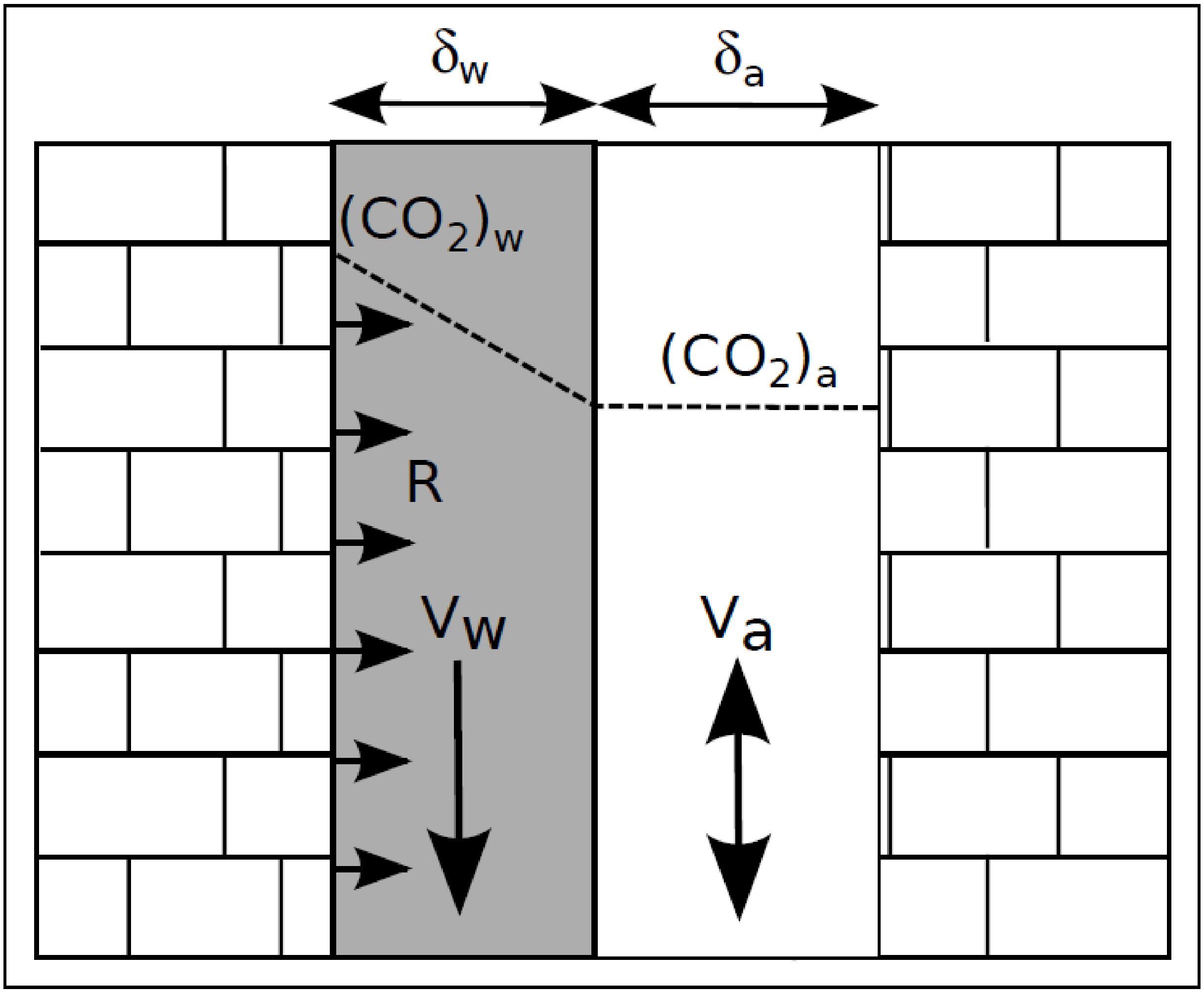

Figure 3. The geometry of the assumed model for transport of CO_2 within the air and water flowing in a fracture given by Equations 13 and 14. The dashed line depicts CO_2 concentration, which is assumed to be uniform across the air-filled cross-section and linear across the water film. Exchange is assumed to be controlled by the rate of diffusion within the water film. *R* depicts the production of CO_2 at the rock-water boundary.

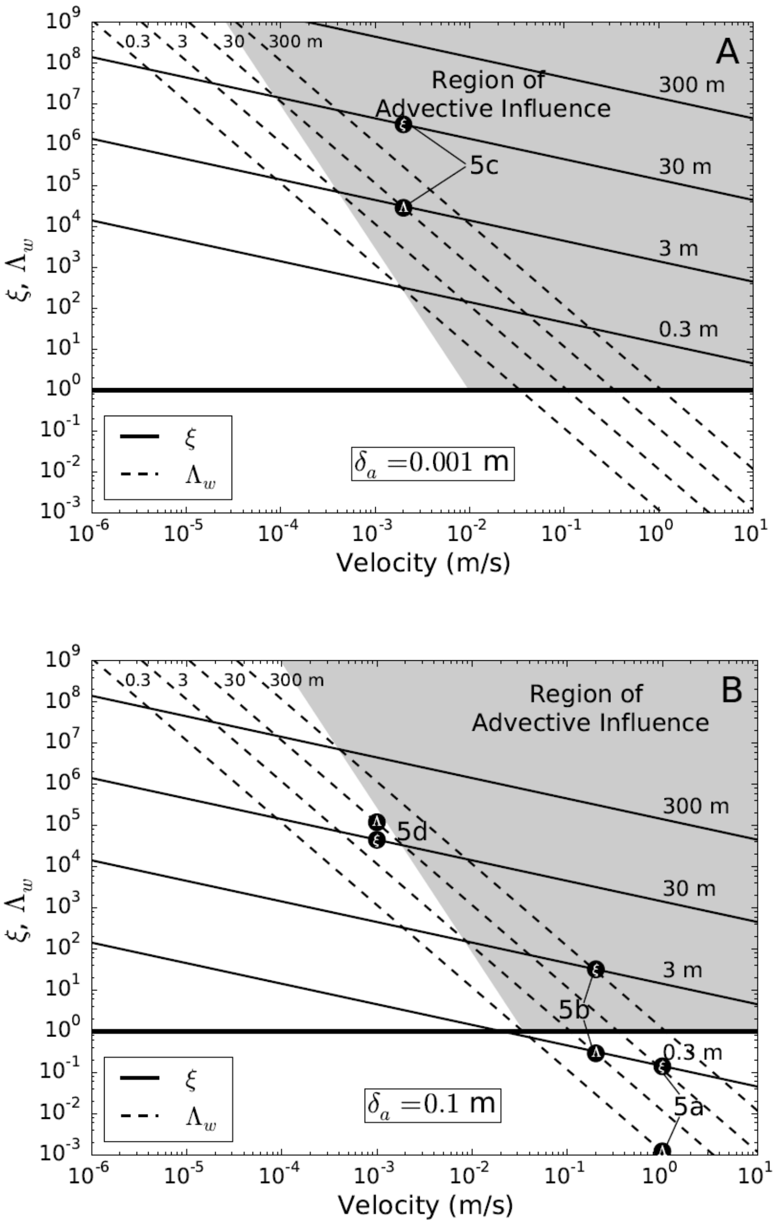

Figure 4. The dimensionless numbers ξ (solid) and Λ_w (dashed) as a function of flow velocity for different values of fracture length (L = 0.3 m, 3 m, 30 m, and 300 m). Advection is important in determining the CO_2 profile with depth when $\xi > 1$ and $\xi > \Lambda_w$ (shaded region). Panel (A) shows a case where the air-filled fracture aperture is 0.001 m, and Panel (B) shows a case where the air-filled fracture aperture is 0.1 m. The letters and numbers (5a-d) label values of ξ and Λ_w for the example profiles shown in Figure 5.

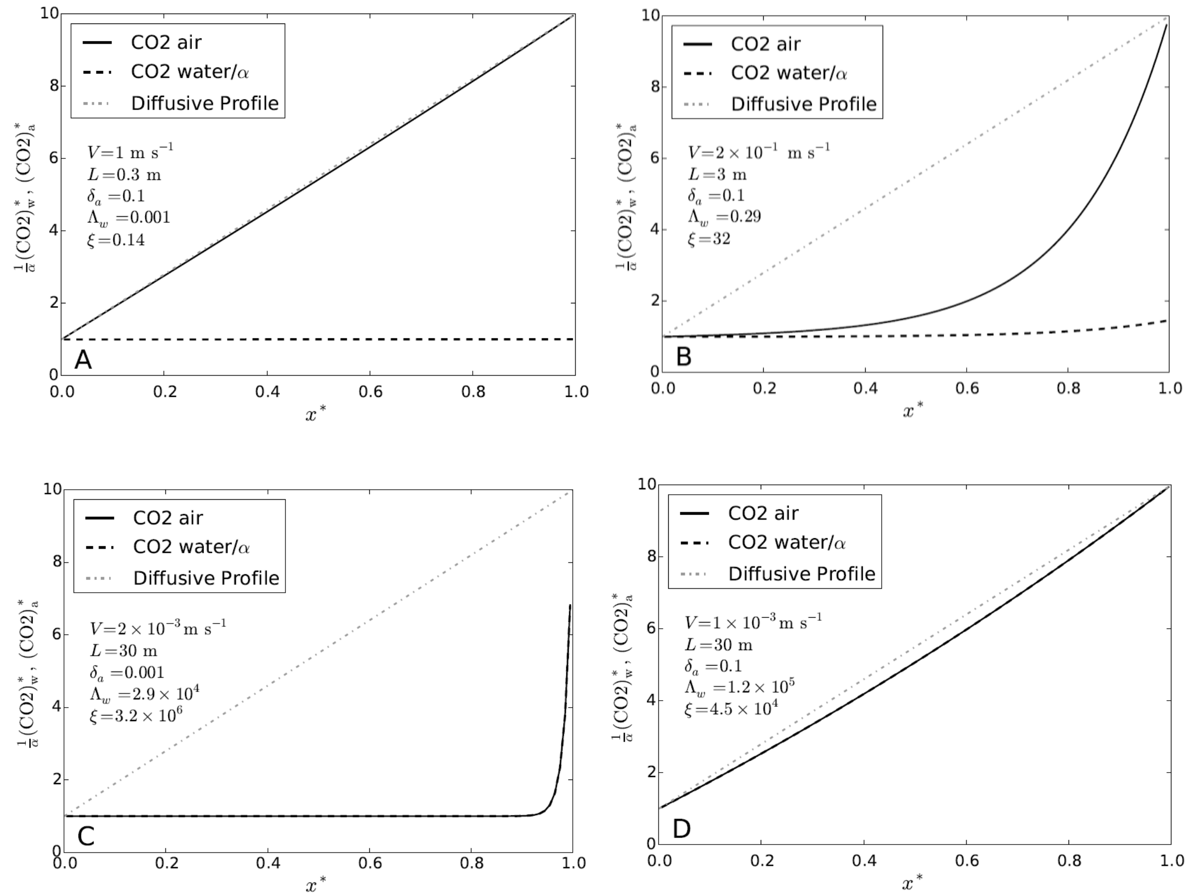

Figure 5. Example profiles of water and air CO_2 with depth in the vadose zone for different choices of parameters as shown in each panel. These examples assume a source of CO_2 at the bottom (X^*=1). The solid line depicts the air CO_2 concentration, the black dashed line depicts the water CO_2 concentration, and the grey dashed line depicts the purely diffusive profile for air CO_2. The location of each case within the parameter space is also depicted in Figure 4. The water film influences the CO_2 air concentration when ξ>1 and ξ>Λ_w. When Λ_w>1 then the CO_2 profile in the water is closely coupled to the CO_2 profile in the air.

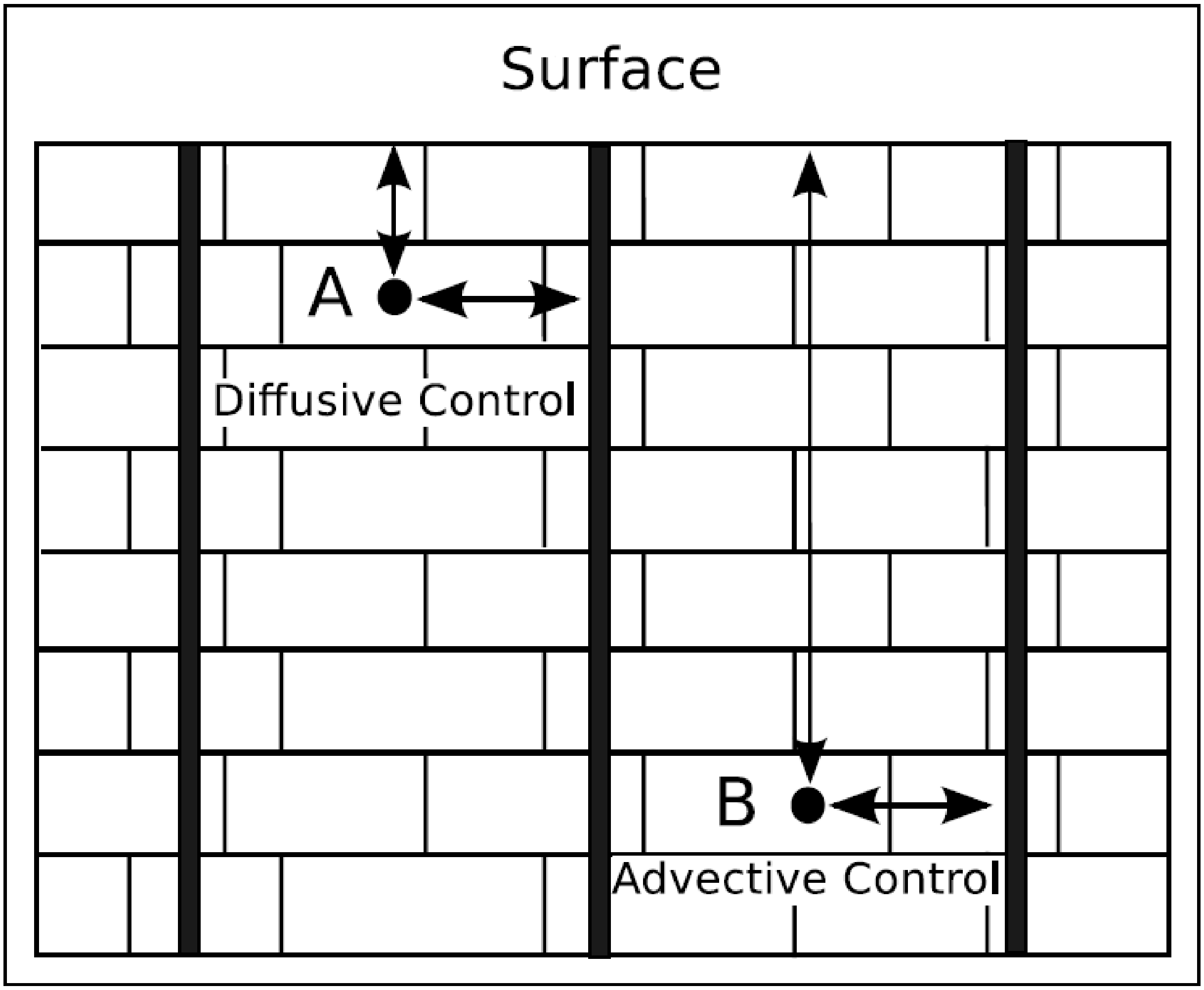

Figure 6. A profile through the vadose zone with three advectively dominated vertical fractures through the rock. At point A, dynamics will be largely controlled by diffusion, because it is as close to the surface as it is to the fractures. However, at point B advection is likely to influence CO_2 concentration, since diffusion to the advective fracture will be much faster than diffusion to the surface. Though much of the vadose zone may not be in close proximity to a fracture flow path dominated by advection, many points within the vadose zone will be closer to such a path than they are to the surface.